Electrically controllable spin states of holes and electrons in organic semiconductor materials

Shohei Iguchi[†], Yuki Sakurai[†], Naohiro Fujita[†], Fumiya Osawa[†] and Kazuhiro Marumoto[*,†,‡]

[†]Division of Materials Science, University of Tsukuba, Tsukuba, Ibaraki 305-8573, Japan

[‡]Tsukuba Research Center for Energy Materials Science (TREMS), University of Tsukuba, Ibaraki 305-8570, Japan

* Correspondence should be addressed to marumoto@ims.tsukuba.ac.jp

ABSTRACT:

Elucidating hole and electron states in organic semiconductor materials is one of the important issues for both their fundamental science and device applications. However, the detailed charge states, in particular, their spin states, have not yet been fully elucidated from a microscopic viewpoint. Here we show electrically controllable spin states of holes and electrons in typical organic semiconductor materials, a polymer regioregular poly(3-hexylthiophene) (RR-P3HT) and a small molecule pentacene, using electron spin resonance (ESR) spectroscopy. Using their ambipolar organic semiconductor devices, these states were revealed as a function of accumulated charge density. The spin states of the electrically accumulated electrons in RR-P3HT and pentacene are clarified for the first time. Moreover, the formation of spinless states of electrons in RR-P3HT and holes in pentacene are demonstrated under high charge density, showing a contrast to the spin states under low charge density. This result would be important for further understating hole and electron states in organic semiconductor materials and for improving the performance of organic semiconductor devices from a microscopic viewpoint.

KEYWORDS: spin states, holes and electrons, organic semiconductors, ambipolar devices, electron spin resonance spectroscopy

1. INTRODUCTION

Organic semiconductor materials and their devices have been attracting much attention because they have advantages such as low cost, large area printability, low environmental impact, and flexibility[1-5]. Among them, ambipolar organic materials can transport both hole and electron carriers in their single devices[6-8]. Thus, if their device structures are optimized, both carriers can be accumulated in a single layer, which can realize a quasi *p*-*n* junction without chemical doping[6,8,9]. Using ambipolar organic transistor structures, the useful devices such as light-emitting organic transistors and complementary metal-oxide semiconductor (CMOS)-like logic circuits have been developed; the CMOS is useful due to the low static power dissipation and the simple circuit design[6,8-10].

Elucidating the hole and electron states in organic semiconductor materials is one of important issues for understanding the operation mechanism and for improving the performance of ambipolar organic semiconductor devices, which may lead to other applications with new functions. To this day, their transport characteristics such as mobility, conductivity, activation energy, etc. have been studied to understand the charge states of ambipolar organic materials, where many important issues such as the difference in charge-carrier balance between holes and electrons and the existence of trapping states depending on materials have been discussed[6-13]. However, the detailed spin states of holes and electrons in organic materials and the

correlation between the spin states and the accumulation characteristics in their devices have not yet been fully investigated from a microscopic viewpoint, which would be important for further understanding and improving ambipolar organic materials and their devices.

Electron spin resonance (ESR) spectroscopy is one of the most effective methods for investigating the spin states of charges in electronic materials and their devices[14-23]. The ESR method measures microwave absorption of unpaired electrons under external magnetic field. The ESR method has an advantage of directly observing charges with spins (unpaired electrons) in the materials and devices nondestructively, and has revealed microscopic properties such as spin and charge states, charge-carrier dynamics, and molecular orientation in the materials and the devices[14-23]. In particular, the spin state of charges is one of the essential natures for characterizing the electronic states of organic semiconductor materials[24,25]. In lightly chemically doped conducting polymers, nonlinear excitations such as solitons and polarons are typical spin/charge carriers reflecting their quasi-one-dimensional structural backbone with strong electron-phonon interactions[24,25]. At higher doping levels, doubly charged spinless bipolarons or a metallic state have been discussed from viewpoints of experimental and theoretical studies[24–27]. The ESR study on a typical high-mobility conducting polymer regioregular poly(3-hexylthiophene) (RR-P3HT) using a device structure has demonstrated that the spin state of electrically accumulated hole carriers clearly changes from a singly positively

charged spin-accompanied state (a positive polaron) under low hole density to a doubly positively charged spinless state (a positive bipolaron or a pair of positive polarons) under high hole density when electrically accumulated hole density increses[17]. However, the spin state of electrically accumulated electrons and its change in RR-P3HT have not yet been investigated. Moreover, for conducting small molecules, not only the spin states of electrically accumulated electrons but also the change of the spin state of electrically accumulated holes and electrons have not yet been studied.

Here we report an ESR study on electrically controllable spin states of holes and electrons in RR-P3HT and a typical high-mobility conducting small molecule pentacene. The RR-P3HT and pentacene are bench mark materials for organic semiconductor transistors because they show high carrier mobilities[1]. This study was carried out using ambipolar organic semiconductor device structures with asymmetric contact electrodes, which revealed the accumulation processes of both holes and electrons and the difference in these spin states in their organic semiconductor materials. Using the ambipolar organic devices, the spin states of electrically accumulated electrons in RR-P3HT and pentacene are firstly observed by ESR. Moreover, the drastic changes of the spin state of electrically accumulated holes and electrons from spin-accompanied to spinless are demonstrated when the charge density in the devices increases.

2. MATERIALS AND DEVICE FABRICATION

A schematic structure of a fabricated device is shown in Figure 1a. To attain high signal-to-noise (S/N) ratio of the ESR signal by increasing the active area of the device, we utilized a rectangular device structure (3×30 mm^2) in an ESR sample tube with an inner diameter of 3.5 mm. Chemical structures of employed organic semiconductor materials RR-P3HT and pentacene are shown in Figure 1b. Thin films of RR-P3HT and pentacene were deposited by a spin-coating method and a vapor-deposition method, respectively. Ion gels were used as an insulator in the present device structure because high charge-density states in the semiconductors with low-voltage device operation can be achieved owing to the formation of electric double layers at the interfaces between the semiconductors and the insulator[10,13,17,18,20,21,23,28-32]. The ion-gel gate insulators can induce very large charge density, which is typically two orders of magnitude larger than that with conventional solid gate insulators[10,13,17,18,20,21,23,28-32]. This is because the distance between ions in ion gels and charges in semiconductors is very short, typically nanometer order, which is typically two orders of magnitude shorter than that with conventional solid gate insulators[10,13,17,18,20,21,23,28-32]. 1-ethyl-3-methylimidazolium bis(trifluoromethylsulfonyl)imide ([EMIM][TFSI]) was used as ionic liquid and poly(styrene-*b*-methylmethacrylate-*b*-styrene) (PS-PMMA-PS) was used as a gelator ABA-type triblock copolymer, and the combination of [EMIM][TFSI] and PS-PMMA-

PS formed ion gels. EMIM and TFSI are cations and anions in the ion gels, respectively. The ion gels are nonmagnetic, which is useful for avoiding back-ground ESR signals[17,18,21,23]. Asymmetric contact electrodes of Au and LiF/Al were utilized to reduce the injection barriers for hole and electron accumulation using the same thin films, respectively[9,13,33]. Contact electrodes of Au (47 nm) and LiF/Al (0.5 nm/46.5 nm) and a gate electrode of Ni/Au (3 nm/47 nm) were deposited by a vapor-deposition method. The fabricated device was sealed into the ESR sample tube in a nitrogen-filled glove box after the device was connected to wires by Ag paste. The ESR measurements were performed at room temperature. Other details concerning the fabrication and evaluation methods are described in Experimental Section.

3. RESULTS AND DISCUSSION

3.1. Operando ESR Spectra of Ambipolar Organic Devices.

Spin states of holes and electrons in the organic semiconductor materials are clearly reflected in the ESR signals. Here we present the ESR signals due to electrically accumulated holes and electrons in the organic semiconductor materials using the devises in positive and negative gate-voltage (V_G) regions, respectively; holes and electrons can be observed separately at different voltages. Figure 2a,b shows the dependence of the ESR spectra of the RR-P3HT and pentacene devices on positive and negative V_G, respectively. Here the asymmetric contact electrodes (Au and Al) were short-circuited with no applied voltage, and the V_G was applied to

these electrodes. In order to carry out stable ESR measurements, we applied the V_G in the range of $|V_G| < 2$ V.

First, we discuss the ESR spectra of the RR-P3HT device at negative V_G in Figure 2a. An ESR signal was already observed at $V_G = 0$ V in this device. A previous ESR study has reported that the signal is ascribed to holes in RR-P3HT molecules due to oxygen doping[34]. In the negative V_G region, the peak-to-peak ESR intensity (I_{pp}) increased with decreasing V_G and showed a maximum at $V_G = -1.0$ V. As discussed later, the number of spins evaluated from the ESR spectra also showed a maximum at $V_G = -1.0$ V. The ESR linewidth increased with decreasing the V_G from $V_G = 0$ V, which is likely caused by the effect of magnetic dipolar interactions among electrically induced holes under high charge density[17]. The ESR parameters at $V_G = -1.0$ V were obtained as the g factor of $g = 2.0025 \pm 0.0001$ and the peak-to-peak ESR linewidth (ΔH_{pp}) of $\Delta H_{pp} = 504 \pm 30$ μT. Here the g factor was extracted from the resonance magnetic field (H_0), where the ESR spectrum with a first derivative form has a value of zero, and the magnetic resonance condition of $h\nu = g\mu_B H_0$, where h is the Planck constant, ν is the frequency of the microwave used in this study, and μ_B is the Bohr magneton. When the V_G further decreased from $V_G = -1.0$ V, the I_{pp} decreased. As discussed later in detail, the decrease is ascribed to the formation of spinless states of electrically accumulated holes under high charge density[17].

In the positive V_G region, the I_{pp} decreased with increasing the V_G and showed a minimum at V_G = +0.3 V as shown in Figure 2a. This result means the de-doping of oxygen-doped holes by electrically accumulated electrons. By further increasing the V_G, the I_{pp} increased and showed a maximum at V_G = +1.5 V. As discussed later, the number of spins evaluated from the ESR spectra showed a maximum at V_G = +1.5 V. It is worth noting that the ESR signal of electrically accumulated electrons has been observed for the first time for ion-gel-gated devices with organic semiconductor materials. This observation may be ascribed to two effects by the high charge-density state due to the ion-gel insulator and by the reduction of electron-injection barriers due to the LiF/Al contact electrode. The ESR parameters at V_G = +1.5 V were obtained as g = 2.0025±0.0001 and ΔH_{pp} = 200±10 μT. Note that the I_{pp} slightly decreased when the V_G further increased from V_G = +1.5 V, which shows the first observation of the formation of spinless state of electrically accumulated electrons in the RR-P3HT device, as discussed later.

Next, we discuss the ESR spectra of the pentacene device at negative V_G in Figure 2b. For the pentacene device, no ESR signal was observed at V_G = 0 V, which shows that the pentacene molecules are not doped with oxygen[14]. In the negative V_G region, the ESR signal due to holes was observed when the V_G decreased below V_G = −0.7 V. The I_{pp} increased by

further decreasing the V_G and showed a maximum at $V_G = -1.0$ V. The ESR parameters at $V_G = -1.0$ V were obtained as $g = 2.0031 \pm 0.0001$ and $\Delta H_{pp} = 51 \pm 3$ μT. These parameters are consistent with those of holes reported for a pentacene transistor[14]. Note that when the V_G further decreased from $V_G = -1.0$ V, the I_{pp} decreased. This behavior has been observed for small molecule ion-gel-gated devices for the first time, which is ascribed to the formation of spinless state of electrically accumulated holes in the pentacene device, as discussed later. In the positive V_G region, the ESR signal due to electrically accumulated electrons was observed above $V_G = +1.8$ V. The I_{pp} monotonically increased with increasing the V_G until $V_G = +2.0$ V. It is worth noting that the ESR signal due to electrically accumulated electrons in pentacene devices has been observed for the first time. As mentioned for the RR-P3HT device, this observation may be ascribed to two effects by the high charge-density state and by the reduction of the injection barrier at the LiF/Al contact electrode. The ESR parameters at $V_G = +1.9$ V were obtained as $g = 2.0031 \pm 0.0001$ and $\Delta H_{pp} = 55 \pm 3$ μT.

3.2. Spin States of Electrically Accumulated Charges

To discuss the spin states of electrically accumulated charges in the organic devices in detail, we evaluated the V_G dependence of the number of spins (N_{spin}) and the number of charge (N_{charge}). The N_{spin} value was evaluated by integrating the ESR spectrum twice and by comparing with the standard Mn^{2+} marker sample. That is, the N_{spin} value was calculated by

the comparison between the double integral values of the ESR spectrum of the device and that of the maker sample with a known N_{spin} value. In this case, the N_{spin} value is proportional to $I_{pp}\times(\Delta H_{pp})^2$. Thus, the N_{spin} includes the effect of the broaden ESR linewidth due to magnetic dipolar interactions among electrically accumulated charges. This broaden ESR linewidth was observed for the RR-P3HT device in negative V_G region as shown in Figure 2a. This observation is due to the larger N_{spin} value compared to other cases as shown in Figure 3, which causes magnetic dipolar interactions among electrically accumulated charges owing to its high spin concentration. In this case, although the I_{pp} is small, the N_{spin} can be large due to the broad ESR linewidth because $N_{spin} \propto I_{pp}\times(\Delta H_{pp})^2$. The N_{charge} value was measured from quasi-static capacitance-voltage (QSCV) characteristics using semiconductor device parameter analyzer, where the voltage between the asymmetric contact electrodes was not applied. Here, the amount of the N_{charge} obtained from the QSCV characteristics means the variation of the number of charges from that at V_G = 0 V, and the state of N_{charge} = 0 at V_G = 0 V may not necessary to be that at the flat-band potential. The N_{charge} for the reverse V_G sweep was not measured because of the experimental difficulty with the QSCV method. If electrically accumulated charges become spinless under high charge density, the N_{spin} is expected to decrease even when the N_{charge} increases. Figure 3a,b shows the V_G dependence of the N_{spin} and N_{charge} of the RR-P3HT and pentacene devices, respectively. For the RR-P3HT device, the N_{charge} monotonically increased as the absolute value of V_G increased in both negative and

positive V_G regions, which indicated that holes and electrons were electrically accumulated in the device monotonically, respectively (see Figure 3a). However, the N_{spin} did not show a monotonic increase. The N_{spin} increased when the absolute value of V_G increased in both negative and positive V_G regions, showing two maxima at $V_G = -1.0$ and +1.5 V, and then started to decrease in higher negative and positive V_G regions, respectively. The decrease in the N_{spin} for $V_G < -1.0$ V can be attributed to the formation of spinless hole states, which is consistent with that of the previous report[17]. It is worth noting that the decrease in the N_{spin} for $V_G > +1.5$ V shows the formation of spinless electron states in RR-P3HT. Thus, these results directly demonstrate that spinless hole and electron states are electrically formed in RR-P3HT under high charge-density conditions separately at different voltages. The doping concentration per a thiophene ring of RR-P3HT for electrically accumulated holes and electrons is evaluated to be ~4.9% and ~0.79% from the N_{spin} of 2.2×10^{14} at $V_G = -1.0$ V and 3.6×10^{13} at $V_G = +1.5$ V using lattice constants[35], respectively, under the assumption of the uniform distribution of spins in the RR-P3HT film under the active area.

For the pentacene device, the N_{charge} showed monotonic increases in both negative and positive V_G regions, as in the case of the RR-P3HT device (see Figure 3b). However, the N_{spin} did not showed a monotonic increase in the negative V_G region. The N_{spin} showed a maximum at $V_G = -1.0$ V, and started to decrease when the V_G further increased for $V_G < -1.0$ V. It is

worth noting that the decrease in the N_{spin} for $V_G < -1.0$ V clearly shows the formation of spinless electrically accumulated holes in pentacene for the first time. Similar formation of spinless holes has been observed for the RR-P3HT device, as mentioned above. Thus, the results of the RR-P3HT and pentacene devices may indicate the formation of spinless holes under high charge-density conditions regardless of molecular structures such as polymers and small molecules. The doping concentration per a pentacene monomer for electrically accumulated holes and electrons is evaluated to be ~1.3% and ~0.64% from the N_{spin} of 4.4×10^{13} at $V_G = -1.0$ V and 2.1×10^{13} at $V_G = +2.0$ V using lattice constants[36], respectively, under the assumption of the uniform distribution of spins in the pentacene film under the active area. The formation of spinless electrically accumulated electrons was not observed in the positive V_G region. This result may be ascribed to low charge density of electrically accumulated electrons owing to the large threshold voltage for the electron accumulation. Figure 1c show the energy diagrams of the highest occupied molecular orbital (HOMO) and lowest unoccupied molecular orbital (LUMO) of RR-P3HT and pentacene with different charge-accumulation process under different applied V_G. As shown in Figure 1c, the energy difference between the LUMO level and the work function of Al is larger for pentacene than that for RR-P3HT[37,38]. This large energy difference causes the large threshold voltage for the electron accumulation in pentacene, which gives rise to small number of electrically accumulated electrons, and week or negligible interactions among the electrons in pentacene.

We here discuss hysteresis behavior for the V_G dependence of the N_{spin} in Figure 3a,b. That is, while the V_G dependence of the N_{spin} showed a maximum for the forward V_G sweep from 0 to −1.5 V, it did not show a maximum for the reverse V_G sweep from −1.5 to 0 V without forming spin states (polarons or radical cations). We have performed several V_G scanning for the same device with RR-P3HT or pentacene thin film. As a result, we have observed reproducible behavior for the N_{spin} of the RR-P3HT and pentacene devices, which denies the degradation of these devices. One of the reasons for this hysteresis behavior may be due to a direct release of spinless charges from the devices. That is, charges are released without separating doubly charged spinless states into singly charged spin states. There are different hysteresis features as shown in Figure 3. That is, the hysteresis for the RR-P3HT device for $V_G < 0$ is larger than that for $V_G > 0$, and the hysteresis trend for the pentacene device for $V_G > 0$ is opposite to those for $V_G < 0$ in the RR-P3HT and pentacene devices. The reason for this difference is not clear at present. One possible reason may be due to strong interactions between holes or electrons in semiconductors and anions or cations in ion gels, respectively. Also, the strength of the interactions may depend on semiconductor molecular structures such as polymers (RR-P3HT, etc.) and oligomers (pentacene, etc.). Another possibility for the hysteresis might be due to the participation of ions from ion gels in ESR. Further investigation into the interactions seems an interesting issue, which is beyond the scope of the present study

and will be reported in a separate paper.

The decreases in the N_{spin} for the RR-P3HT and pentacene devices under both high positive and negative V_G regions indicate the formation of the spinless charge states. That is, the spin states of electrically accumulated charges dramatically change from spin-accompanied to spinless when the $|V_G|$ value increases. At lower doping level, spin-accompanied excitations such as polarons are typical spin/charge carriers in organic semiconductor materials[24,25], which have been demonstrated by the ESR studies using organic semiconductor devices with conventional solid gate insulator[14-16,34]. However, at higher doping level, spinless excitations such as bipolarons and pairs of polarons are typical doubly-charged carriers in organic semiconductor materials[24,25,39,40]. A bipolaron or a pair of polarons are stabilized by stronger electron-phonon interactions than Coulomb interactions as discussed in theoretical studies[39,40]. The formation of a pair of *same charged* polarons has been theoretically discussed and demonstrated, where the crossover between a polaron and a bipolaron *via* the formation of a pair of polarons has been pointed out when doping concentration is increased[39,40]. For the pair of polarons, a spin singlet state is stabilized compared to a spin triplet state owing to an antiferromagnetic exchange interaction between the polarons[39,40]. For the bipolaron, a spin singlet state is stabilized due to an occupation of antiparallel spins at the same energy level[39,40]. In the cases of solution samples under high doping levels, the formation of a bipolaron (a

dication) in oligomers such as oligo-thiophene has been experimentally reported using optical and ESR methods[41,42]. Also, the formation of spinless charges has been shown by the ESR study for holes in the RR-P3HT device with the ion-gel gate insulator[17]. In the present study, electrically controllable spin states of holes and electrons in the RR-P3HT and pentacene devices have been demonstrated, which shows the formation of spinless charge states under high charge-density conditions.

3.3. DFT Analysis of Electrically Accumulated Charges and Molecular Orientation

The spin states of electrically accumulated holes and electrons can be further investigated from a theoretical viewpoint, which is useful for analyzing the experimental results. The density functional theory (DFT) calculation was performed to study the *g* factors and the spin density distribution of the present organic semiconductor meterials[43]. Figure 4a,b shows the chemical structures of a thiophene heptamer (7T) and a pentacene monomer for the DFT calculations, respectively, where the 7T is used as a model molecule of RR-P3HT. The DFT calculations were performed for radical cationic and anionic states of the isolated 7T and pentacene monomers using the Gaussian 09 software package with the UB3LYP functional and the basis sets of 6-31G(d,p) for calculations of cations and 6-31+G(d,p) for calculations of anions, respectively, where these monomer structures have been optimized for the charged states[43]. The *g* factors of holes in thin films of RR-P3HT and pentacene have been

theoretically and experimentally studied using the DFT method[44,45]. The DFT calculations of the isolated monomers have reproduced the experimentally observed *g* factors of the organic thin films, which may indicate that the *g* factors of the organic thin films are primarily determined by molecular orbitals of the isolated monomers due to relatively weak van der Waals-type molecule-molecule interactions[44,45]. Figure 4c-f show the calculated spin density distribution of 7T and pentacene for cationic and anionic states, respectively. We defines the coordinate axes in Figure 1b and 4a,b as the *x*-axis is parallel to the short axis of the molecules, the *y*-axis is parallel to the long axis of the molecules, and the *z*-axis is perpendicular to the molecular planes, respectively. Table 1 summarizes the principal values of the calculated *g* tensors. The orthorhombic anisotropy of the *g* tensors has been obtained for both 7T and pentacene.

It is interesting to compare the experimental results with the theoretical calculations. For the RR-P3HT device, the *g* factors of the ESR signals of electrically accumulated holes in RR-P3HT were measured as $g = 2.0023$-2.0026 depending on the V_G. It is well known that RR-P3HT has an edge-on orientation due to the formation of a lamellar structure[1,17]. In this case, the direction of the *x*-axis is perpendicular to the substrate plane, which is parallel to the *H* direction in the present ESR measurement, where the corresponding *g* factor is calculated as $g_x = 2.0029$ from the DFT calculation (see Table 1). The observed *g* factors of electrically

accumulated holes can be basically explained by the edge-on orientation of the lamellar structure; a small decrease in the *g* factors of 0.0003-0.0006 from the theoretical value may be explained by the orientation distribution of molecules in RR-P3HT films[34]. Also, there are large differences between the calculated *g* factors and spin density distribution of the cationic and anionic states of 7T, which are clearly shown by an average of the principal values g_{avg} in Table 1 and Figure 4c,e, respectively. These differences can be explained by the violation of charge-conjugation symmetry (CCS) due to the existence of sulfur hetero atoms (see Figure 1b and 4a)[46-48]. For the case of electrically accumulated electrons, the observed *g* factor varied in the range of $g = 2.0023$-2.0025 depending on the V_G. The observed *g* factor is considerably smaller than the calculated $g_x = 2.0039$ for the *x*-axis direction with a difference of 0.0014-0.0016, and is relatively close to the calculated $g_z = 2.0019$ for the *z*-axis direction with a difference of 0.0004-0.0006. Thus, this result may point out a possibility that electrically accumulated electrons exist at the sites where molecules tend to have a face-on orientation with the *z*-axis is perpendicular to the substrate plane. The different molecular sites for the hole and electron accumulation may be explained by the variation in the energy levels of HOMO and LUMO of RR-P3HT on the molecular orientation[38,49]. The electron accumulation on the molecules with the face-on orientation may be related to lower mobility of electrons than that of holes in RR-P3HT[1].

Previous works of RR-P3HT molecular orientation have showed that the orientation of lamellar structure is highly dependent on the formation of thin film, and in spin-coated films with low regioregularity of P3HT the lamellae are mostly parallel to the substrate[50,51]. To obtain the information of the molecular orientation further, we have performed X-ray diffraction (XRD) measurements of our spin-coated thin films. As a result, we have observed the XRD data with a peak at 5.4°, which corresponds to the formation of edge-on lamellar structure with an interlayer spacing of 16.4 Å (see the inset of Figure 3a). This result is consistent with the previous studies for RR-P3HT with high regioregularity[50,51,52]; we used the RR-P3HT with high regioregularity in the present study. We have also confirmed the formation of the edge-on lamellar structure with a similar fabrication method used in the present work [17]. However, we did not observe XRD data corresponding to the formation of face-on orientation. This result may indicate that there are no large crystal grains with the face-on orientation in our thin films. While XRD structure analysis may be unsuitable for detecting a very small number of molecules with face-on orientation, the ESR method may be able to indicate the existence of the face-on oriented molecules using anisotropic *g* factors.

For the pentacene device, the *g* factors of the ESR signals of electrically accumulated holes and electrons in pentacene were measured as $g = 2.0031$, which hardly depended on the V_G. It has been reported that pentacene molecules have an edge-on orientation in thin films,

where the *y*-axis is perpendicular to the substrate plane[1,14,36]. For the *y*-axis direction, the *g* factor of the cationic state is calculated as g_y = 2.0030 from the DFT calculation (see Table 1). This result is fully consistent with the observed *g* factor of *g* = 2.0031 for electrically accumulated holes within the experimental error of 0.0001, which indicates that electrically accumulated holes exist at the sites with the edge-on molecular orientation. For the case of electrically accumulated electrons, the *g* factor of *g* = 2.0031 was observed. This value is slightly larger than the calculated *g* factor of g_y = 2.0028 for the *y*-axis direction, and is rather consistent with the calculated *g* factor of g_x = 2.0031 for the *x*-axis direction. Thus, this result may point out a possibility that electrically accumulated electrons exist at the sites where molecules tend to have an edge-on orientation with the *x*-axis direction perpendicular to the substrate plane. The different molecular sites for the hole and electron accumulation may be explained by the variation in the energy levels of HOMO and LUMO of pentacene on the molecular orientation, as discussed above[38,49]. The electron accumulation on the molecules with the different edge-on orientation may be related to lower mobility of electrons than that of holes in pentacene[8]. The difference between the calculated *g* factors of the cationic and anionic states of pentacene is relatively small (see Table 1), which is reasonably explained by the CCS without no hetero atom in the pentacene molecule[46-48]. For the RR-P3HT and pentacene devices, further experiments by measuring a rotation pattern of the *g* factor are needed to fully analyze the molecular orientation, which are currently in progress and will be

reported in a separate paper.

We comment on the transistor characteristics of the present devices. Stable p-type transistor operation has been observed for the RR-P3HT polymer devices, as reported in the previous study[17]. However, stable n-type transistor operation could not be observed with the present devices using the ion gel and organic semiconductors. Also, stable p-type transistor operation could not be observed for the pentacene oligomer devices. The possible reason for unstable n-type operation may be due to strong interactions between cations (EMIM) in the ion gel and electron carriers, which may prevent stable electron transport. Also, strong interactions between anions (TFSI) in the ion gel and hole carriers in oligomer pentacene may prevent stable p-type transistor operation. In our study, even if electrons or holes cannot be transported owing to the strong interactions between cations (EMIM) or anions (TFSI) and electrons or holes, respectively, the ESR method can observe the spin states of the electrons or holes. This is the difference between the charge observations with the transport and ESR methods.

We have performed the ESR studies of organic devices with conventional solid gate insulators without ion gels[14,15,16,34,53]. However, we could not observe a high charge-density state showing a maximum peak in the V_G dependence of the N_{spin} as shown in Figure 3. The

reason has been ascribed to low charge density in the devices with conventional solid gate insulators. As demonstrated in Figure 3 of the present study, the use of ion gels can achieve high charge-density states showing a maximum peak in the V_G dependence of the N_{spin}. The uses of different concentration of ionic liquid in ion gels and/or different ionic liquid in ion gels are interesting topics, which are currently in progress and will be reported in a separate paper.

4. CONCLUSIONS

Our results present the spin states of electrically accumulated holes and electrons and their molecular states in the devices with the typical organic semiconductor materials RR-P3HT and pentacene using the ESR technique and the DFT calculations. The formation of spinless holes and electrons in RR-P3HT and holes in pentacene is demonstrated under high charge densities regardless of the molecular structures; the spinless charge formation is one of the interesting physical properties under high charge densities[24]. This information is also useful for precisely evaluating the charge mobility in organic semiconductor devices under high charge density because the mobility cannot be precisely evaluated without determining the amount of electric charge for a charge carrier. The spinless charge formation may contribute to high charge mobility due to the decrease in spin scatterings between charges, as discussed in the ESR studies of carbon materials such as carbon nanotubes and graphene[21,23]. The electrically controllable spin states may be applied to produce novel spintronics because the

magnetic degree of freedom of a charge carrier plays a crucial role in spintronics. Our results would be important for further understating charge states in ambipolar organic semiconductor materials and may be useful for improving the performance of ambipolar organic semiconductor devices from a microscopic viewpoint. Our method is general and can be applicable to the elucidation of charge states in other organic semiconductor materials.

5. EXPERIMENTAL SECTION

5.1. Fabrication of ambipolar organic devices. The devices were fabricated using two types of nonmagnetic substrates; one was a polyethylene terephthalate (PET) film with dimensions of 30 mm × 3 mm × 100 μm (Mitsubishi Polyester Film, Inc.), and the other was a quartz glass with dimensions of 30 mm × 3 mm × 1 mm (IIYAMA PRECISION GLASS Co, Ltd.). Gate electrodes of Ni/Au (3/47 nm) were vapor-deposited on the PET substrate using an ULVAC VPC-260F vacuum evaporation system. Ion-gel solutions consisted of an ionic liquid, 1-ethyl-3-methylimidazolium bis(trifluoromethylsulfonyl) imide ([EMIM][TFSI]) (52.2 wt%) (Ionic Liquids Technologies, Inc.), a gelator ABA-type triblock copolymer poly(styrene-*b*-methylmethacrylate-*b*-styrene) (PS-PMMA-PS) (4.3 wt%) (Polymer Source, Inc.), and a solvent ethyl acetate (43.5 wt%) (Wako Pure Chemical Industries, Ltd.); the mixture was stirred for over one and half day, drop-casted on the gate electrode and then thermally annealed at 70 °C under vacuum for over one and half day. The polymer layers were fabricated by spin-

coating a RR-P3HT (Sigma-Aldrich Co. LLC., regioregularity > 95% head-to-tail) solution with chlorobenzene as the solvent (Nacalai Tesque, Inc.) on the quartz substrate. After spin-coating the RR-P3HT solution, the RR-P3HT thin films were thermally annealed at 70 °C under vacuum for 30 min. The film thickness was approximately 90 nm. The pentacene layers with a film thickness of 100 nm were vapor-deposited on the quartz substrate using an ULVAC VPC-260F vacuum evaporation system under 5×10^{-4} Pa. The asymmetric contact electrodes of Au (47 nm) and LiF/Al (0.5/46.5 nm) were fabricated with a vapor-deposition method on the organic thin films, which had a channel length of 0.5 mm and a channel width of approximately 23 mm. Finally, the PET substrate with the gate electrode was placed on the quartz substrate with the organic layer and the contact electrodes, completing the device fabrication. The fabricated device was sealed into an ESR sample tube after the device was connected to wires by Ag paste in a nitrogen-filled glove box (O_2 < 0.4 ppm, H_2O < 0.5 ppm).

5.2. Device characterization. The ESR measurements were performed with a JEOL RESONANCE JES-FA200 X-band ESR spectrometer and a Keithley 2612A source meter. The ESR signals were measured as a function of V_G by averaging the ESR spectrum over typically 10–30 min. The *g* factor and the linewidth of the ESR signals were calibrated using a standard Mn^{2+} marker sample. The peak-to-peak ESR linewidth (ΔH_{pp}) was evaluated as the difference between the two magnetic fields at a peak and valley in the ESR spectrum. The

number of spins (N_{spin}) was evaluated by integrating the ESR spectrum twice and by comparing it with that of the Mn^{2+} marker sample. The absolute value of the N_{spin} of the Mn^{2+} marker sample was calculated using a solution (220 μL) of 4-hydroxy-2,2,6,6-tetramethylpiperidin-1-oxyl (TEMPOL) as a standard. The calibration of the *g* factor was performed using a software program from the JEOL RESONANCE ESR system considering high second-order correction to the effective resonance field. Its correctness was also confirmed using 2,2-diphenyl-1-picrylhydrazyl (DPPH) as another standard sample.

The quasi-static capacitance-voltage (QSCV) measurements were performed with an Agilent B1500A semiconductor device parameter analyzer. The number of charges (N_{charge}) were evaluated by integrating a steady-state current in the devices for time, which were measured as a function of V_G.

The X-ray diffraction (XRD) measurements were performed with a PANalytical X'Pert Pro MPD powder diffractometer equipped with a rapid counting system (X'Celerator). The X-ray beam was nickel-filtered Cu Kα (λ = 1.5418 Å) radiation from a sealed tube with a horizontal line focus operated at 45 kV and 40 mA.

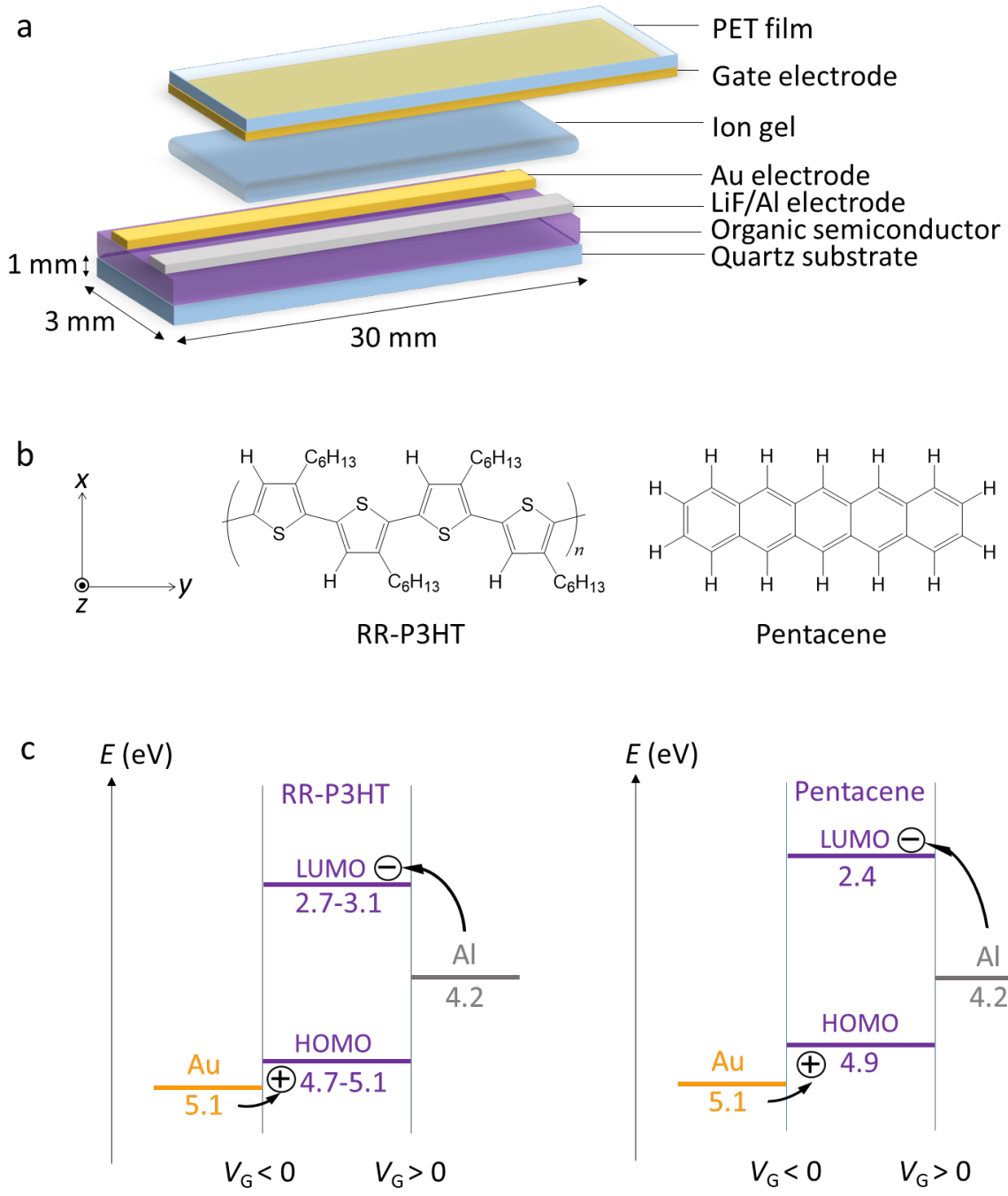

Figure 1. Schematic of an organic device and the organic materials, and their energy diagrams. (a) Schematic structure of an organic semiconductor device used in this study. (b) Chemical structures of the organic semiconductor material RR-P3HT and pentacene. The definitions of the coordinate axes of RR-P3HT and pentacene molecules are shown. (c) Energy diagrams of the HOMO and LUMO of RR-P3HT and pentacene with different charge-accumulation process under different applied gate voltage (V_G).

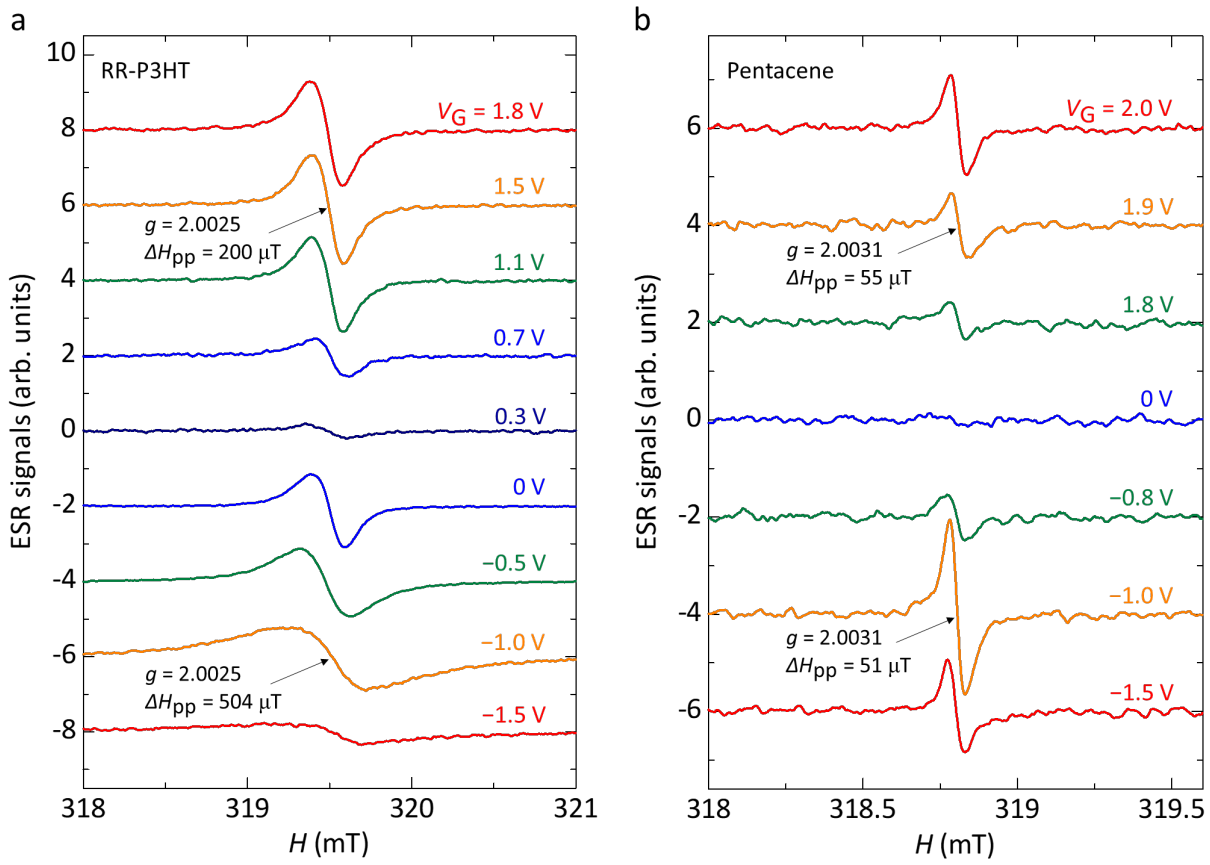

Figure 2. Dependence of the ESR spectra of the organic devices on the gate voltage. (a) The ESR spectra of the RR-P3HT device at positive and negative gate voltage (V_G) at the external magnetic field H perpendicular to the substrate ($H_\perp$) at room temperature (RT), where the voltage between the asymmetric contact electrodes was not applied. (b) The ESR spectra of the pentacene device at positive and negative V_G at the $H_\perp$ at RT, where the voltage between the asymmetric contact electrodes was not applied.

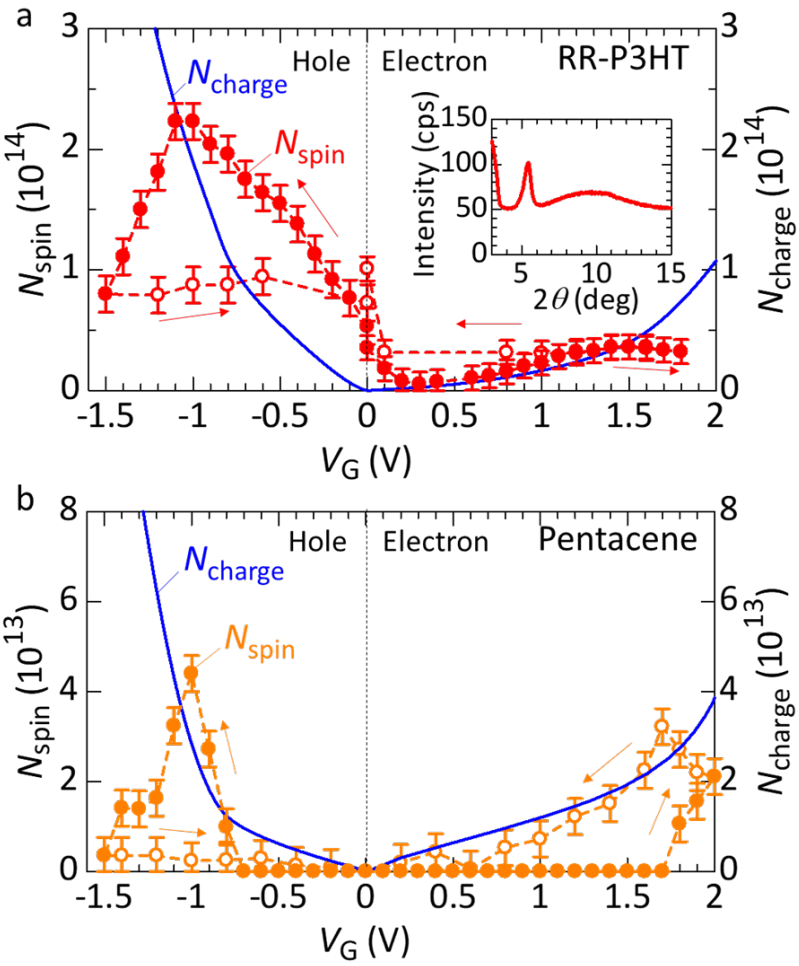

Figure 3. The number of spins (N_{spin}) and the number of charges (N_{charge}) of the organic devices. (a) The V_G dependence of the N_{spin} and N_{charge} of the RR-P3HT device at $H_\perp$ at RT, where the voltage between the asymmetric contact electrodes was not applied. The inset shows the data of X-ray diffraction for a RR-P3HT thin film. (b) The V_G dependence of the N_{spin} and N_{charge} of the pentacene device at the $H_\perp$ at RT, where the voltage between the asymmetric contact electrodes was not applied. In (a) and (b), solid and open symbols denote the data for forward and reverse V_G sweeps, respectively.

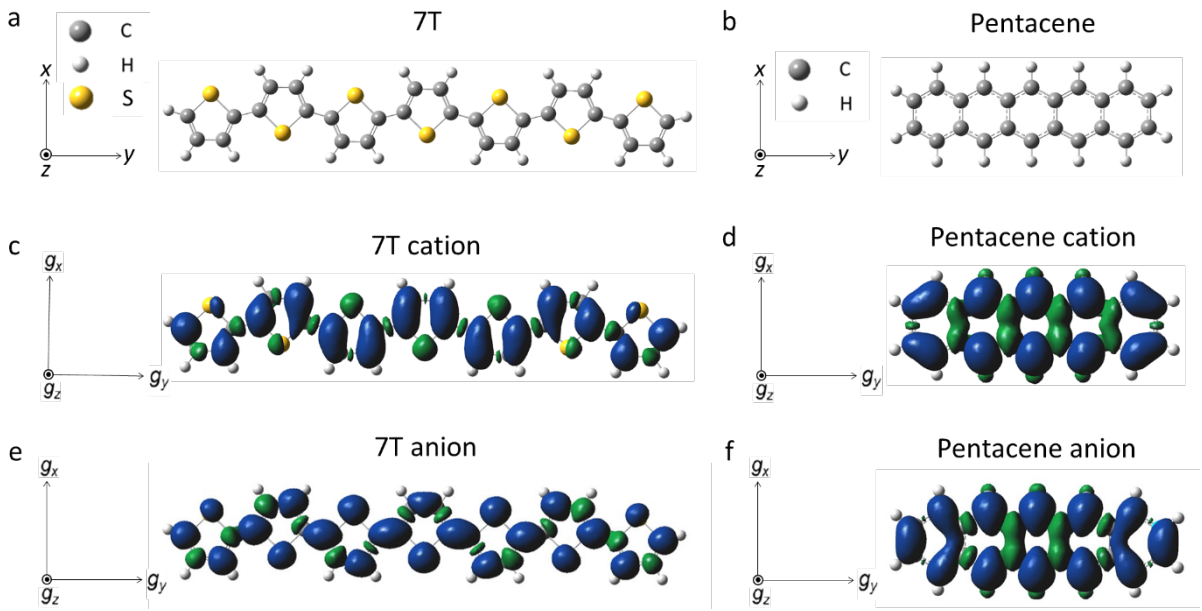

Figure 4. Chemical structures and the DFT calculations of a model molecule of RR-P3HT and pentacene. (a,b) Chemical structures of a thiophene heptamer (7T) (a) and a pentacene monomer (b) used for the DFT calculations. The definitions of the coordinate axes of 7T and pentacene molecules are shown. **c-e**, The spin density distribution of 7T (c,e) and pentacene (d,f) for cationic states (c,d) and anionic states (e,f) obtained from the DFT calculations. The directions of the principal axes of the calculated *g* tensors are shown.

Table 1. Principal values of calculated g tensors g_i ($i = x, y, z$) and the averaged g factor g_{avg} for 7T and pentacene. Principal values of the calculated g tensor g_i ($i = x, y, z$) were obtained from the DFT calculations for 7T and pentacene. An average of the principal values g_{avg} was calculated as $g_{avg} = \sqrt{g_x^2\langle l^2\rangle + g_y^2\langle m^2\rangle + g_z^2\langle n^2\rangle}$ using $l = \sin\theta\cos\varphi$, $m = \sin\theta\sin\varphi$, and $n = \cos\theta$, where $< >$ represents spatial average. Here random orientation of molecules was assumed to calculate the g_{ave}.

molecule	charge state	g_x	g_y	g_z	g_{avg}
7T	cation	2.0029	2.0008	2.0021	2.0019
7T	anion	2.0040	2.0087	2.0019	2.0049
Pentacene	cation	2.0026	2.0030	2.0024	2.0027
Pentacene	anion	2.0031	2.0028	2.0016	2.0025

AUTHOR INFORMATION

Corresponding Author

*E-mail: marumoto@ims.tsukuba.ac.jp

Notes

The authors declare no competing financial interests.

1. Acknowledgements

This work was partially supported by JSPS KAKENHI Grant Number JP15K13329, by JST PRESTO, by The Murata Science Foundation, by The Hitachi Global Foundation, and by JST ALCA Grant Number JPMJAL1603, Japan.

REFERENCES

(1) Dimitrakopoulos, C. D.; Malenfant, P. R. L. Organic Thin Film Transistors for Large Area Electronics. *Adv. Mater.* **2002**, *14*, 99-117.

(2) Sakai, S.; Soeda, J.; Häusermann, R.; Matsui, H.; Mitsui, C.; Okamoto, T.; Ito, M.; Hirose, K.; Sekiguchi, T.; Abe, T.; Uno M.; Takeya, J. All Solution-Processed Organic Single-Crystal Transistors with High Mobility and Low-Voltage Operation. *Org. Electron.* **2015**, *22*, 1-4.

(3) Wu, X.; Ma, Y.; Zhang, G.; Chu, Y.; Du, J.; Zhang, Y.; Li, Z.; Duan, Y.; Fan, Z.; Huang, J. Thermally Stable, Biocompatible, and Flexible Organic Field-Effect Transistors and Their Application in Temperature Sensing Arrays for Artificial Skin. *Adv. Funct. Mat.* **2015**, *25,* 2138-2146.

(4) Matsuhisa, N.; Kaltenbrunner, M.; Yokota, T.; Jinno, H.; Kuribara, K.; Sekitani, T.; Someya, T. Printable Elastic Conductors with a High Conductivity for Electronic Textile Applications. *Nat. Commun.* **2015***, 6*, 7461.

(5) Yamashita, Y. Organic Semiconductors for Organic Field-Effect Transistors. *Sci. Technol. Adv. Mater.* **2009**, *10*, 024313.

(6) Muccini, M. A Bright Future for Organic Field-Effect Transistors. *Nat. Mater.* **2006**, *5,* 605-613.

(7) Zhao, Y.; Guo, Y.; Liu, Y. 25th Anniversary Article: Recent Advances in n-Type and Ambipolar Organic Field-Effect Transistors. *Adv. Mater.* **2013**, *25,* 5372-5391.

(8) Meijer, E. J.; De Leeuw, D. M.; Setayesh, S.; Van Veenendaal, E.; Huisman, B.-H.; Blom, P. W. M.; Hummelen, J. C.; Scherf, U.; Klapwijk, T. M. Solution-Processed Ambipolar Organic Field-Effect Transistors and Inverters. *Nat. Mater.* **2003**, *2,* 678-682.

(9) Zaumseil, J.; Friend, R. H.; Sirringhaus, H. Spatial Control of the Recombination Zone in an Ambipolar Light-Emitting Organic Transistor. *Nat. Mater.* **2006**, *5*, 69-74.

(10) Kim, S.-H.; Hong, K.; Xie, W.; Lee, K.-H.; Zhang, S.; Lodge, T. P.; Frisbie, C. D. Electrolyte-Gated Transistors for Organic and Printed Electronics. *Adv. Mater.* **2013**, *25*, 1822-1846.

(11) Sciascia, C.; Martino, N.; Schuettfort, T.; Watts, B.; Grancini, G.; Antognazza, M. R.; Zavelani-Rossi, M.; McNeill, C. R.; Caironi, M. Sub-Micrometer Charge Modulation Microscopy of a High Mobility Polymeric n-Channel Field-Effect Transistor. *Adv. Mater.* **2011**, *23*, 5086-5090.

(12) Ha, T.-J.; Sonar, P.; Cobb, B.; Dodabalapur, A. Charge Transport and Density of Trap States in Balanced High Mobility Ambipolar Organic Thin-Film Transistors. *Org. Electron.* **2012**, *13*, 136-141.

(13) Yomogida, Y.; Pu, J.; Shimotani, H.; Ono, S.; Hotta, S.; Iwasa, Y.; Takenobu, T. Ambipolar Organic Single-Crystal Transistors Based on Ion Gels. *Adv. Mater.* **2012**, *24*, 4392-4397.

(14) Marumoto, K.; Kuroda, S.; Takenobu, T.; Iwasa, Y. Spatial Extent of Wave Functions of Gate-Induced Hole Carriers in Pentacene Field-Effect Devices as Investigated by Electron Spin Resonance. *Phys. Rev. Lett.* **2006**, *97*, 256603.

(15) Marumoto, K.; Arai, N.; Goto, H.; Kijima, M.; Murakami, K.; Tominari, Y.; Takeya, J.; Shimoi, Y.; Tanaka, H.; Kuroda, S. Microscopic Mechanisms Behind the High Mobility in Rubrene Single-Crystal Transistors as Revealed by Field-Induced Electron Spin Resonance. *Phys. Rev. B.* **2011**, *83*, 075302.

(16) Tanaka, H.; Hirate, M.; Watanabe, S.; Kaneko, K.; Marumoto, K.; Takenobu, T.; Iwasa, Y.; Kuroda, S. Electron Spin Resonance Observation of Charge Carrier Concentration in Organic Field-Effect Transistors During Device Operation. *Phys. Rev. B.* **2013**, *87*, 045309.

(17) Tsuji, M.; Takahashi, Y.; Sakurai, Y.; Yomogida, Y.; Takenobu, T.; Iwasa, Y.; Marumoto, K. Two-Dimensional Magnetic Interactions and Magnetism of High-Density Charges in a Polymer Transistor. *Appl. Phys. Lett.* **2013**, *102*, 133301.

(18) Takahashi, Y.; Tsuji, M.; Yomogida, Y.; Takenobu, T.; Iwasa, Y.; Marumoto, K. Electron Spin Resonance Study of Organic Interfaces in Ion Gel-Gated Rubrene Single-Crystal Transistors. *Appl. Phys. Express* **2013**, *6*, 041603.

(19) Tanaka, H.; Hirate, M.; Watanabe, S.; Kuroda, S. Microscopic Signature of Metallic State in Semicrystalline Conjugated Polymers doped with Fluoroalkylsilane Molecules. *Adv. Mater.* **2014**, *26*, 2376-2383.

(20) Nagasaki, Y.; Lee, J.-H.; Kubozono, Y.; Kambe, T. Dynamics of Carrier Injection in Picene Thin-Film Field-Effect Transistors with an Ionic Liquid Sheet and Ionic Liquid Gel. *Org. Electron.* **2014**, *15*, 3070-3075.

(21) Matsumoto, D.; Yanagi, K.; Takenobu, T.; Okada, S.; Marumoto, K. Electrically Induced Ambipolar Spin Vanishments in Carbon Nanotubes. *Sci. Rep.* **2015**, *5*, 11859.

(22) Kang, K.; Watanabe, S.; Broch, K.; Sepe, A.; Brown, A.; Nasrallah, I.; Nikolka, M.; Fei, Z.; Heeney, M.; Matsumoto, D.; Marumoto K.; Tanaka H.; Kuroda S.; Sirringhaus H. 2D Coherent Charge Transport in Highly Ordered Conducting Polymers Doped by Solid State Diffusion. *Nat. Mater.* **2016**, *15*, 896-902.

(23) Fujita, N.; Matsumoto, D.; Sakurai, Y.; Kawahara, K.; Ago, H.; Takenobu, T.; Marumoto, K. Direct Observation of Electrically Induced Pauli Paramagnetism in Single-Layer Graphene Using ESR Spectroscopy. *Sci. Rep*. **2016**, *6*, 34966.

(24) Heeger, A. J.; Kivelson, S.; Schrieffer, J.-R.; Su, W.-P. Solitons in Conducting Polymers. *Rev. Mod. Phys.* **1988**, *60*, 781-850.

(25) Helmut G. Kiess (Ed). Conjugated Conducting Polymers. *Springer-Verlag Berlin Heiderberg*, **1992**.

(26) Lee, K. Cho; Park, S.-H.; Heeger, A. J.; Lee, C.-W.; Lee S.-H. Metallic Transport in Polyaniline. *Nature* **2006**, *441*, 65-68.

(27) Sai, N.; Li, Z.-Q.; Martin, M. C.; Basov, D. N.; Ventra, M. D. Electronic Excitations and Metal-Insulator Transition in Poly(3-hexylthiophene) Organic Field-Effect Transistors. *Phys. Rev. B* **2007**, *75*, 045307.

(28) Yuen, J. D.; Dhoot, A. S.; Namdas, E. B.; Coates, N. E.; Heeney, M.; McCulloch, I.; Moses, D.; Heeger, A. J. Electrochemical Doping in Electrolyte-Gated Polymer Transistors. *J. Am. Chem. Soc.* **2007**, *129*, 14367-14371.

(29) Panzer, M. J.; Frisbie, C. D. Polymer Electrolyte-Gated Organic Field-Effect Transistors: Low-Voltage, High-Current Switches for Organic Electronics and Testbeds for Probing Electrical Transport at High Charge Carrier Density. *J. Am. Chem. Soc.* **2007**, *129*, 6599-6607.

(30) Cho, J.-H.; Lee, J.; He, Y.; Kim, B.; Lodge, T. P.; Frisbie, C. D. High-Capacitance Ion Gel Gate Dielectrics with Faster Polarization Response Times for Organic Thin Film Transistors. *Adv. Mater.* **2008**, *20*, 686-690.

(31) Cho, J.-H.; Lee, J.; Xia, Y.; Kim, B.; He, Y.; Renn, M. J.; Lodge, T. P.; Frisbie, C. D. Printable Ion-Gel Gate Dielectrics for Low-Voltage Polymer Thin-Film Transistors on Plastic. *Nat. Mater.* **2008**, *7*, 900-906.

(32) Du, H.; Lin, X.; Xu, Z.; Chu, D. Electric Double-Layer Transistors: a Review of Recent Progress. *J. Mater. Sci*. **2015**, *50*, 5641-5673.

(33) Yamane, K.; Yanagi, H.; Sawamoto, A.; Hotta, S. Ambipolar Organic Light Emitting Field Effect Transistors with Modified Asymmetric Electrodes. *Appl. Phys. Lett.* **2007**, *90*, 162108.

(34) Marumoto, K.; Muramatsu, Y.; Nagano, Y.; Iwata, T.; Ukai, S.; Ito, H.; Kuroda, S.; Shimoi, Y.; Abe, S. Electron Spin Resonance of Field-Induced Polarons in Regioregular Poly(3-alkylthiophene) Using Metal–Insulator–Semiconductor Diode Structures. *J. Phys. Soc. Jpn.* **2005**, *74*, 3066-3076.

(35) Joshi, S.; Grigorian, S.; Pietsch, U. X-ray Structural and Crystallinity Studies of Low and High Molecular Weight Poly(3-hexylthiophene). *Phys. Status Solidi A* **2008**, *205*, 488-496.

(36) Yoshida, H.; Inaba, K.; Sato, N. X-ray Diffraction Reciprocal Space Mapping Study of the Thin Film Phase of Pentacene. *Appl. Phys. Lett.* **2007**, *90*, 181930.

(37) Nagamori, T.; Marumoto, K. Direct Observation of Hole Accumulation in Polymer Solar Cells During Device Operation Using Light-Induced Electron Spin Resonance. *Adv. Mater.* **2013**, 25, 2362-2367.

(38) Yoshida, H.; Yamada, K.; Tsutsumi, J.; Sato, N. Complete Description of Ionization Energy and Electron Affinity in Organic Solids: Determining Contributions from

Electronic Polarization, Energy Band Dispersion, and Molecular Orientation. *Phys. Rev. B* **2015**, *92*, 075145.

(39) Shimoi, Y.; Abe, S. Competition between Polarons and Bipolarons in Nondegenerate Conjugated Polymers. *Phys. Rev. B* **1994**, *50*, 14781-18784.

(40) Shimoi, Y.; Kuwabara, M.; Abe, S. Highly Doped Nondegenerate Conjugated Polymers - A Theory Using the DMRG Method. *Synth. Met.* **2001**, *119*, 213-214.

(41) Fichou, D.; Horowitz, G.; Xu, B.; Garnier, F. Stoichiometric Control of the Successive Generation of the Radical Cation and Dication of Extended π-Conjugated Oligothiophenes: A Quantitative Model for Doped Polythiophene. *Synth. Met.* **1990**, *39*, 243-259.

(42) Iwasa, T.; Kawai, T.; Onoda, M.; Nakayama, J.; Nakahara, H.; Yoshino, K. In Situ Absorption Spectra and ESR Measurements of Poly(trans-(2,2'-bithiophene-5-yl)-(2,2':5',2''-terthiophene-5-yl)ethylene) During Electrochemical Doping. *J. Phys. Soc. Jpn.* **1992**, *61*, 666.

(43) Frisch, M. J.; Trucks, G. W.; Schlegel, H. B.; Scuseria, G. E.; Robb, M. A.; Cheeseman, J. R.; Scalmani, G.; Barone, V.; Mennucci, B.; Petersson, G. A.; Nakatsuji, H.; Caricato, M.; Li, X.; Hratchian, H. P.; Izmaylov, A. F.; Bloino, J.; Zheng, G.; Sonnenberg, J. L.; Hada, M.; Ehara, M.; Toyota, K.; Fukuda, R.; Hasegawa, J.; Ishida, M.; Nakajima, T.; Honda, Y.; Kitao, O.; Nakai, H.; Vreven, T.; Montgomery, Jr., J. A.; Peralta, J. E.; Ogliaro, F.; Bearpark, M.; Heyd, J. J.; Brothers, E.; Kudin, K. N.; Staroverov, V. N.; Kobayashi, R.;

Normand, J.; Raghavachari, K.; Rendell, A.; Burant, J. C.; Iyengar, S. S.; Tomasi, J.; Cossi, M.; Rega, N.; Millam, J. M.; Klene, M.; Knox, J. E.; Cross, J. B.; Bakken, V.; Adamo, C.; Jaramillo, J.; Gomperts, R.; Stratmann, R. E.; Yazyev, O.; Austin, A. J.; Cammi, R.; Pomelli, C.; Ochterski, J. W.; Martin, R. L.; Morokuma, K.; Zakrzewski, V. G.; Voth, G. A.; Salvador, P.; Dannenberg, J. J.; Dapprich, S.; Daniels, A. D.; Farkas, Ö.; Foresman, J. B.; Ortiz, J. V.; Cioslowski, J.; Fox, D. J. Gaussian 09, Revision D.01, Gaussian, Inc., Wallingford CT, **2013**.

(44) Shimoi, Y.; Marumoto, K.; Kuroda, S. Theoretical ESR *g* Values in Rubrene and Oligoacenes: Implication to Molecular Orientation at Interfaces in Organic FETs. *Mol. Cryst. Liq. Cryst.* **2012**, *566*, 33-37.

(45) Son, D.; Kuwabara, T.; Takahashi, K.; Marumoto, K. Direct Observation of UV-induced Charge Accumulation in Inverted-Type Polymer Solar Cells with a TiO_x Layer: Microscopic Elucidation of the Light-Soaking Phenomenon. *Appl. Phys. Lett.* **2016**, *109*, 133301.

(46) Swanson, L. S.; Shinar, J.; Yoshino, K. Optically Detected Magnetic Resonance Study of Polaron and Triplet-Exciton Dynamics in Poly(3-hexylthiophene) and Poly(3-dodecylthiophene) Films and Solutions. *Phys. Rev. Lett.* **1990**, *65*, 1140-1143.

(47) Swanson, L. S.; Shinar, J.; Lane, P. A.; Hess, B.; Wudl, F. Optically Detected Magnetic Resonance (ODMR) of Polarons and Charge-Conjugation Symmetry in Conducting Polymers. *Synth. Met*. **1992**, *49-50*, 481-489.

(48) Shinar, J.; Swanson, L. S. Optically Detected Magnetic Resonance (ODMR) Studies of Conducting Polymers: An Overview. *Synth. Met*. **1992**, *49-50*, 621-630.

(49) Heimel, G.; Salzmann, I.; Duhm, S.; Rabe, J. P.; Koch, N. Intrinsic Surface Dipoles Control the Energy Levels of Conjugated Polymers. *Adv. Funct. Mater.* **2009**, *19*, 3874-3879.

(50) Sirringhaus, H.; Brown, P. J.; Friend, R. H.; Nielsen, M. M.; Bechgaard, K.; Langeveld-Voss, B. M. W.; Spiering, A. J. H.; Janssen, R. A. J.; Meijer, E. W.; Herwig, P.; de Leeuw, D. M. Two-dimensional charge transport in self-organized, high-mobility conjugated polymers. *Nature* **1999**, *401*, 685-688.

(51) Österbacka, R.; An, C. P.; Jiang, X. M.; Vardeny, Z. V. Two-Dimensional Electronic Excitations in Self-Assembled Conjugated Polymer Nanocrystals. *Science* **2000**, *287*, 839-842.

(52) Chen, T.-A.; Wu, X.; Rieke, R. D. Regiocontrolled Synthesis of Poly(3-alkylthiophenes) Mediated by Rieke Zinc: Their Characterization and Solid-State Properties *J. Am. Chem. Soc.* **1995**, *117*, 233.

(53) Marumoto, K.; Muramatsu, Y.; Ukai, S.; Ito H.; Kuroda, S. Electron Spin Resonance Observations of Field-Induced Polarons in Regioregular Poly(3-octylthiophene) Metal-Insulator-Semiconductor Diode Structures. *J. Phys. Soc. Jpn.* **2004**, *73*, 1673-1676.

Table Of Contents (TOC) graphic